



HAL
open science

Carbide-Free Bainite Transformations Above and Below Martensite Start Temperature Investigated by In-Situ High-Energy X-Ray Diffraction

Cécile Rampelberg, Sébastien Yves Pierre Allain, Guillaume Geandier, Julien
Teixeira, Florimonde Lebel, Thomas Sourmail

► **To cite this version:**

Cécile Rampelberg, Sébastien Yves Pierre Allain, Guillaume Geandier, Julien Teixeira, Florimonde Lebel, et al.. Carbide-Free Bainite Transformations Above and Below Martensite Start Temperature Investigated by In-Situ High-Energy X-Ray Diffraction. JOM Journal of the Minerals, Metals and Materials Society, 2022, 73, pp.3181-3194. 10.1007/s11837-021-04903-8 . hal-03391108

HAL Id: hal-03391108

<https://hal.univ-lorraine.fr/hal-03391108>

Submitted on 28 Nov 2022

HAL is a multi-disciplinary open access archive for the deposit and dissemination of scientific research documents, whether they are published or not. The documents may come from teaching and research institutions in France or abroad, or from public or private research centers.

L'archive ouverte pluridisciplinaire **HAL**, est destinée au dépôt et à la diffusion de documents scientifiques de niveau recherche, publiés ou non, émanant des établissements d'enseignement et de recherche français ou étrangers, des laboratoires publics ou privés.



Distributed under a Creative Commons Attribution 4.0 International License

Carbide-free bainite transformations above and below Martensite Start temperature investigated by in-situ High-Energy X-Ray Diffraction

Cécile Rampelberg^{1,2}, Sébastien Yves Pierre Allain¹, Guillaume Geandier¹, Julien Teixeira¹, Florimonde Lebel¹, Thomas Sourmail²

¹ Institut Jean Lamour, UMR CNRS UL 7198, Campus ARTEM, 2 Allée André Guinier, 54000 Nancy, France ; cecile.rampelberg@univ-lorraine.fr; sebastien.allain@univ-lorraine.fr; guillaume.geandier@univ-lorraine.fr; julien.teixeira@univ-lorraine.fr; florimonde.lebel@univ-lorraine.fr

² Ascometal CREAS, Swiss Steel Group, BP 70045, Hagondange, France; thomas.sourmail@ascometal.com

Corresponding author : Cécile Rampelberg cecile.rampelberg@univ-lorraine.fr

Abstract

Carbide-Free Bainitic AHSS exhibit multiphase microstructures made of fine ferrite and retained austenite. The carbon partition between these constituting phases during the bainitic transformation is studied above and below M_s by in-situ High Energy X-Ray Diffraction experiments. The time-resolved analysis of the phase fraction, austenite lattice parameter and ferrite tetragonality offer the possibility to establish phase-scaled consistent and precise carbon balances.

In the studied steel, the carbon content in ferrite ranges between 0.1 and 0.15 wt.% after isothermal treatments meaning that the available carbon for austenite stabilization is reduced. The stasis conditions are close to the T_0' criterion below 400 °C but are not reached at higher temperatures. Our multi-step experiments also prove that the transformation below M_s is very sensitive to the carbon content in austenite and auto-catalytic nucleation processes inherited from prior transformations (martensite and bainite at higher temperature). The bainitic transformation thus does not follow additivity rules.

Keywords: steel; bainite; carbon; synchrotron; tetragonality; multi-step

Introduction

Carbide-Free Bainites (CFB) are multiphase microstructures obtained from austenite decomposition at low temperatures (typically between 450 °C and 300 °C) in alloyed steels which have a high potential for industrial applications [1–6]. They are made of a fine ferritic matrix with a lath morphology without carbide, retained austenite stabilized by carbon partitioning during the transformation and fresh martensite appearing during the final cooling after bainite transformation [1]. Such metastable microstructure can be obtained as the CFB transformation is displacive and incomplete [3,7–9]. The high fraction of residual austenite may transform during further mechanical loading at room temperature (stress or strain induced transformation) and leads to a possible TRIP effect (TRansformation Induced Plasticity) [3,10–14]. These microstructures have been investigated for over 20 years but the criterion for the incomplete transformation phenomenon remains one of the current bones of contention in the literature [15]. Diffusionless theories of bainite transformation assume a thermodynamic limit called the T_0' line (nucleation controlled) [13,16]. During the transformation, the austenite gets progressively enriched by the carbon rejected by the bainitic ferrite. In the so-called “diffusionless” approach, at a given temperature, the nucleation of new bainite units stops when the carbon concentration in austenite exceeds a critical value corresponding to the composition for which both austenite and ferrite have the same Gibbs’s energy. This mechanism leads to an incomplete transformation or a stasis. The T_0 line is the locus of these critical carbon concentration in austenite as a function of the temperature. Thermodynamically, the

formation of bainitic ferrite without change of carbon composition is no more possible when the T_0 temperature goes below the transformation temperature. The T_0' curve takes also into account of the elastic strain energy stored in ferrite (ca. $400 \text{ J}\cdot\text{mol}^{-1}$) in the Gibb's energy calculation [13]. Whereas diffusive theories consider a stagnant process (dissipative mobility of interfaces) during isothermal holding (growth controlled) [17]. The objective of this work is to bring new experimental evidences to feed this discussion; in particular, we will establish very precise carbon balance between phases and challenge the T_0' criterion.

In this work, we have studied the formation of CFB microstructures at different temperatures in isothermal conditions from a fully austenitic state by in-situ High Energy X-Ray Diffraction (HEXRD) experiments. If the transformation occurs above the martensite start temperature (M_s), the final microstructure is composed of bainite (noted B), retained austenite (noted A) and fresh martensite (noted FM). It is far more difficult to study the bainitic transformation below M_s as the martensitic transformation occurs almost instantaneously, prior to the bainitic ones. The final microstructure in that case contains also tempered martensite (TM).

In order to investigate how the initial austenite state affects the transformation below M_s , two multi-step treatments have been designed. Instead of studying the transformation after a partial martensitic transformation, such treatments investigate it after partial bainitic or bainitic/martensitic transformations.

For such transformations, in-situ HEXRD experiments allow for simultaneous measurements of phase transformation kinetics, austenite lattice parameter changes, and evolution of bainitic phase tetragonality all along an uninterrupted isothermal treatments. In addition, minor carbide precipitation processes can be identified [18]. As a consequence, rigorous carbon balance between phases can be established especially in isothermal conditions above M_s . To the knowledge of the authors, this is the first time that such level of consistency is obtained between the estimation of the carbon content in austenite and the carbon kept in supersaturation in bainite [19]. The microstructures after thermal treatments have also been studied by Scanning Electron Microscopy. By coupling these observations, it was possible to finely estimate the stability of retained austenite at room temperature after the different cooling schedules.

Experimental procedure

The studied industrial steel is produced by Ascometal [20] and has a base chemical composition of Fe-0.27C-1.5Mn-1.2Si-0.8Cr (wt.%). For the investigated samples are cylindrical with a size of 10 mm length and 4 mm diameter. Each sample is machined from the mid-radius of a hot-rolled steel bar ($\varnothing 40 \text{ mm}$).

The in-situ HEXRD experiments were performed on the P07 beamline at PETRA III at Deutsches Elektronen-Synchrotron (DESY), Hamburg, Germany. A synchrotron X-Ray monochromatic beam ($500 \times 500 \mu\text{m}^2$) with a high energy (100 keV corresponding to a wavelength $\lambda = 0.123984 \text{ \AA}$) was used to illuminate the sample and to work in transmission in a powder diffraction configuration. The high photon flux from the synchrotron source and the large 2D detector (Perkin-Elmer) with slow and fast acquisition mode, allow collection of Debye-Scherrer diffraction patterns at different rates (10 Hz or 0.3 Hz respectively). The sample was heated with a Bähr DIL 805 A/D dilatometer. The temperature was measured with a thermocouple welded directly on the cylindrical specimen.

In this paper, different thermal conditions were studied: conventional isothermal holdings and multi-step conditions. Multi-step cooling sequences are a succession of isothermal holdings at different decreasing temperatures. All these thermal treatments started with an austenitic soaking at $3 \text{ }^\circ\text{C/s}$ up to $1150 \text{ }^\circ\text{C}$ for 3 minutes leading to a Prior Austenite Grain (PAG) size around $74 \pm 42 \mu\text{m}$ close to that

achieved after hot forging of relatively large components such as automotive crankshafts, wheel hubs, etc. The transition between all the isothermal temperature steps is performed at 50 °C/s.

Figure 1 a) shows the temperature as a function of time schedules for isothermal conditions, with temperatures ranging between 300 °C and 475 °C and holding time is set up at 20 minutes. The investigation of bainite transformation was made below and above the M_s (Martensite start temperature); as the M_s of the alloy is about 350 °C (346 °C) as determined by dilatometry experiment. Using calculations of the M_s in the literature as proposed by Van Bohemen [21] and Nehrenberg [22] we found 356 °C and 333 °C respectively. Those results are closed and in agreement with the one determined experimentally. Above M_s and at M_s , the experiments are denoted by the letter B followed by the transformation temperature. At 300 °C (below M_s), the martensite fraction prior to bainite transition was estimated by the Koistinen-Marburger relation around 61 wt.% [23]. The corresponding experiment will further denoted M+B300. The experiments above M_s will further be denoted as BXXX (XXX = 350, 400, 450 or 475). Isothermal holdings are followed by a cooling down to room temperature.

Figure 1 b) shows the heat treatments corresponding to the multi-step cooling sequences discussed above. The two-step schedule consists in a first step at 400 °C during 40 seconds, followed by a second step at 300 °C during 20 minutes. During the first step, a partial bainitic transformation at 400 °C is expected (typically 30 wt.% of bainite). As the stabilization of austenite is not sufficient in such conditions, a partial martensitic transformation occurs during the transition between the steps. Finally, a bainitic transformation should occur in the untransformed austenite at 300 °C. The designed microstructure is composed of bainite, martensite and bainite at 300 °C. The experiment will be denoted B+M+B300 in the following.

The three-step cooling sequence aimed at studying the bainitic transformation at 300 °C after a well developed bainitic transformations at higher temperatures. Here, a sufficient enrichment of retained austenite is expected to avoid any martensitic transformation. It consists in a first step at 475 °C during 115 seconds then a second step and third step at 400 °C and 300 °C respectively during 20 minutes at each step. The designed microstructure is thus composed of two types of bainite and bainite at 300 °C. The experiment will be denoted B+B300 in the following. As for isothermal holdings, both multi-step conditions are followed by a final cooling to room temperature with a cooling rate of 50 °C/s.

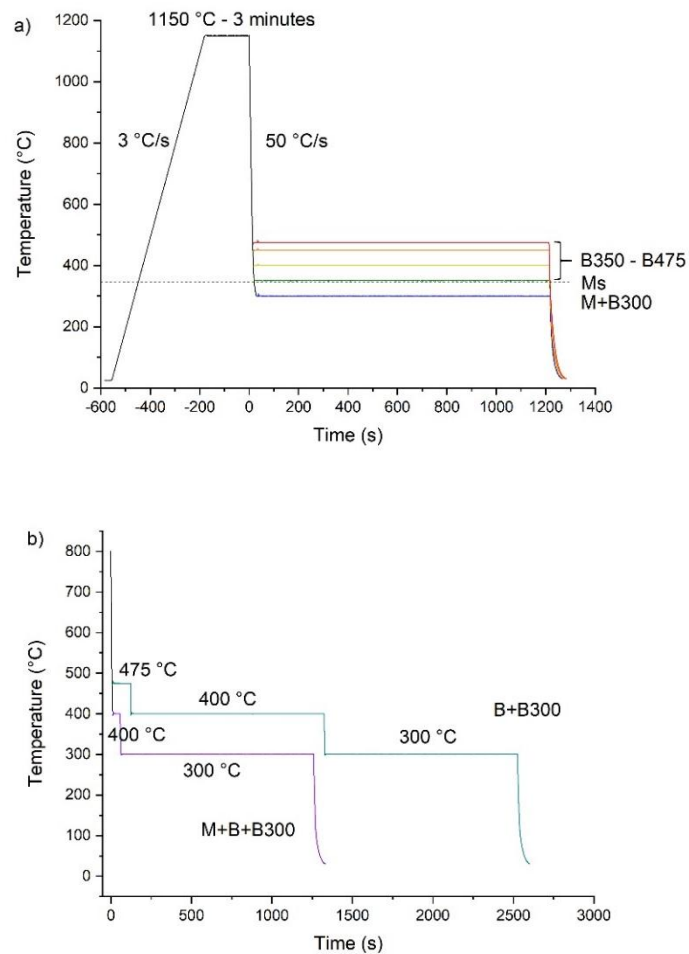


Figure 1: Heat treatments schedules a) isothermal conditions b) multi-step conditions.

The two-dimensional X-Ray patterns obtained during experiments were integrated circularly with the *PyFAI* python library [24]. Sample to detector distance and detector orthogonality to the beam had been calibrated using LaB6 powder (NIST 660a). The one-dimensional diffractograms were analyzed following a Rietveld [25] refinement method using *FullProf* [26]. The pseudo-Voigt function was used in the Rietveld refinement to simulate diffraction peaks. In this refinement, two phases were considered: austenite with a cubic face centered structure (Fm-3m) and bainite and martensite with a body-centered tetragonal structure (I/4 mmm). The R-factor was used for each phase as the indicator of the quality of simulation [27]. During the present experiments, it was not possible to discriminate between these last two phases on the basis of diffraction patterns. The mass fraction of BCT phase thus corresponds to the sum of the bainite and martensite contribution. However, as they appear sequentially, their respective transformation kinetics can be identified uniquely by a metallurgical reasoning on the basis of existing knowledge.

It must be mentioned that the BCT structure systematically leads to a better adjustment than a BCC (Body-Centered Cubic) structure. This has already been observed in previous studies by some groups [28–32]. This justifies the use of a tetragonal unit cell to assess the carbon content in solid solution in bainitic ferrite (in absence of tempered martensite of course).

For all experiments, the mean austenitic grain size is $74 \pm 42 \mu\text{m}$ at high temperature and are thus large compared to the studied volume ($500 \times 500 \times 4000 \mu\text{m}^3$). In the two-dimensional X-rays patterns, the Debye Scherrer rings are discontinuous and exhibit many spots shown in Figure 2 a) as a consequence. These spots affect the austenite peak shapes on the 1D diffractograms shown in Figure 2 b). It is therefore impossible to determine the evolution of the austenite phase with good accuracy from the high temperature and at the very beginning of the bainite transformation. These spots jeopardize not only the correct measurement of the phase fraction but also the austenite lattice parameters. The value becomes exploitable only after a certain amount of bainite transformation. The detection threshold makes possible to after quantification 15 wt.% of bainite transformation only.

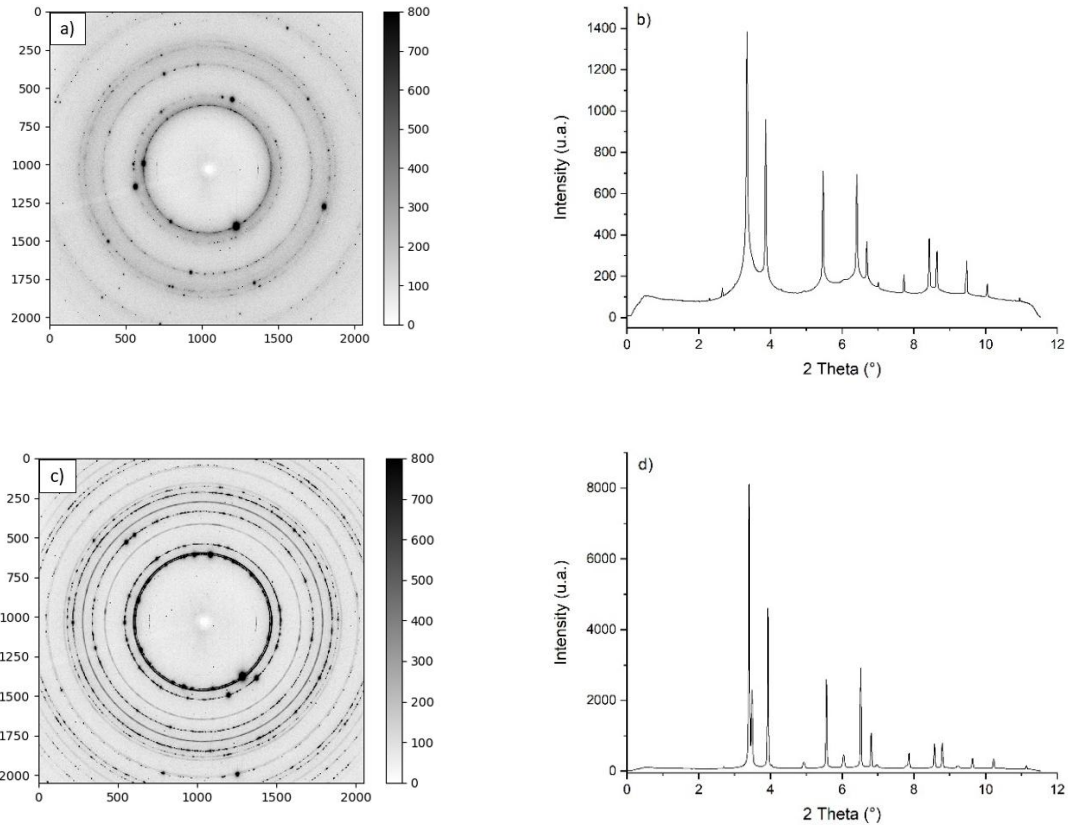


Figure 2 : 2D Image a) and 1D spectrum b) at the end of the austenitic soaking; 2D Image c) and 1D spectrum at the beginning of bainite formation.

Figure 2 c) shows the two-dimensional image for the isothermal experiment at $400 \text{ }^\circ\text{C}$ after the formation of 20 wt.% bainite. The Debye Scherrer rings are still discontinuous and some spots are present and disturb the intensity. However, the position and the intensity of the peaks become insensitive to the apparition or the disappearance of single spots. At this stage shown in Figure 2 d), it was considered that the determined values are meaningful and relevant. The R factor is slightly high (around 2.0) then as the transformation continues the R factor decreases.

Results

Kinetics of bainite and martensite transformation in isothermal conditions

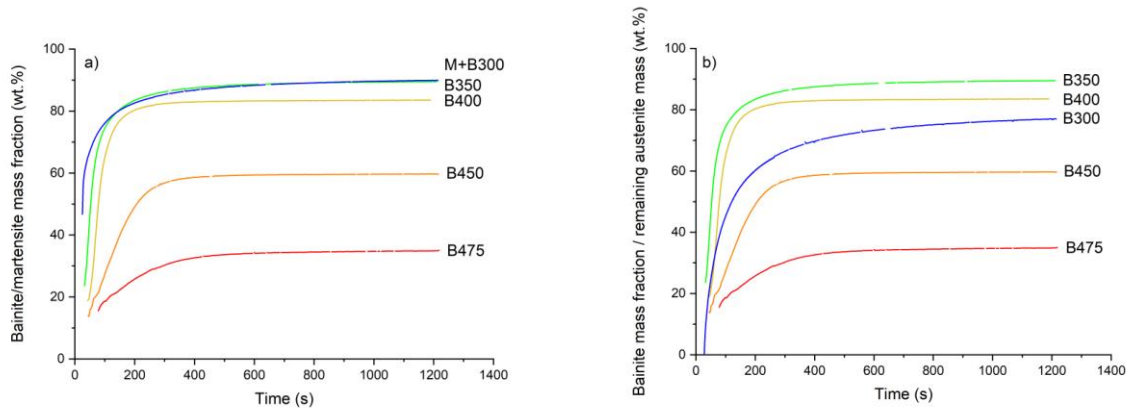


Figure 3 : a) Bainite and martensite mass fraction as a function of time during isothermal holdings ; b) Normalized Bainite mass fraction as a function of time in austenite along isothermal holdings (The normalization procedure is explained in the text). Compared to Figure 3 a), only B300 experiment has been corrected.

Figure 3 a) shows the evolution of bainite and martensite mass fraction as a function of time during isothermal holding at different transformation temperatures between 300 °C and 475 °C measured by HEXRD. The mass fractions are the direct output of the Rietveld refinement procedure based on the absorption coefficients of atoms lattices. The reference time ($t = 0$) was set at the end of the austenitization for all experiments. Bainite mass fractions as a function of time are shown for the duration of isothermal holding and do not include potential changes during final cooling to room temperature.

For isothermal holding above M_s (350 °C and above), the bainite mass fraction increases as a function of time (above 350 °C). Bainite formation kinetics exhibit a sigmoidal curve and do not reach a full transformation. The maximum fraction of bainite formed strongly decreases with increasing isothermal temperature, this is consistent with well established incomplete transformation phenomenon in the presence of Si additions [2,33]. The higher the temperature, the lower the initial transformation rate and the lower the transformed fraction when then the plateau is reached. For the B350 experiment, the slope at the end of the treatment remains significant meaning that the transformation is not strictly finished (the stasis is probably not reached). [9]

The isothermal transformation at 300 °C occurs below the M_s temperature. The kinetics of M+B300 experiment presented in Figure 3 b) are thus the sum of two contributions; first, a martensitic transformation followed by a bainitic one. In order to compare the bainite transformation rate only in austenite, kinetics have been normalized to consider only the transformation of austenite remaining after the martensitic transformation (between M_s and 300 °C, corresponding to a fraction of $F_M = 56$ wt.%). Figure 3 b) shows the normalized kinetics for the different isothermal treatments as a function of time. The normalized bainite mass fraction F_B is calculated as equation 1 :

$$F_B = \frac{F_{M+B} - F_M}{F_A} \quad (1)$$

where F_{M+B} , F_M and F_A are respectively the total mass fraction of BCT phases (data from Figure 3), the mass fraction of martensite and austenite prior to the bainite transformation.

When comparing the normalized results, the rate of bainite transformation at 300 °C is slower than the one obtained at 350 °C [33,34]. There still a controversy about the nature of time dependent transformation observed in such alloys below M_s temperature [34]. The nature of the final product is claimed to be bainitic or martensitic. Some authors as Kim et al. [35] statute that is an athermal martensitic transformation. However, some authors as Van Bohemen et al. [36] consider that the final product as bainite. In our article, the isothermal transformation below M_s is also considered as a bainite transformation.

Nevertheless, this bainitic nucleation is strongly affected by the prior martensitic transformation in the sense that it provides new nucleation sites for bainite, stimulating the autocatalytic nucleation processes at martensite/austenite interface as reported by Ravi et al. [37] by example. The accelerating effect of a prior martensitic transformation often observed in the literature is not put in evidence in our experiment of M+B300 [37]. The bainite fraction reached at the end of the experiment M+B300 is 77 wt.%, lower than the fraction obtained at stasis for B400. For B350, the stasis of the transformation is obviously not achieved as the slope remains significant. Nevertheless, data obtained for isothermal transformation at 300 °C (M+B300) will be used in later discussion of multi-step experiments.

When cooling the samples down to room temperature, fresh martensite (FM) can be formed if austenite is not sufficiently stabilized by carbon partitioning. Table I shows the final composition of the microstructures. The martensitic transformations during final cooling start at temperature lower than expected by the local M_s temperature. Moreover, due to the possible distribution of carbon in between austenite islands, it is more difficult to detect correctly the begin of the transformation which is more sluggish in this latter case. The M_s calculated using the experimental carbon content determined by HEXRD experiments have been reported now the Table I for the sake of comparison the M_s temperature calculated and predicted in the last columns of Table I below were obtained using the empirical formula Van Bohemen [21] and Steven & Haynes [38]. The fraction of FM drastically increases with holding temperature, at the expense of the fraction of austenite reported in Figure 3 b). The highest value of retained austenite fraction at room temperature is obtained after a transformation in B400 in the investigated conditions.

For isothermal transformations at 400 °C and below, the fresh martensite fraction formed at the end of the thermal treatment is low (close to zero wt.%). This is consistent with a greater austenite carbon enrichment at these temperatures. For isothermal transformations at 450 °C, a significant fraction of martensite forms during final cooling, consistent with a M_s temperature well above room temperature (lesser austenite carbon enrichment).

Table I : Phases fractions at room temperature in isothermal conditions measured by HEXRD and the M_s calculated using [21] and [38].

Isothermal temperature (°C)	Bainite (wt.%)	Retained Austenite (wt.%)	Fresh martensite (wt.%)	M_s calculated (°C) [21]	M_s calculated (°C) [38]
350	90	10	0	140	29
400	83	16	1	148	43
450	60	13	27	257	218
475	35	7	58	317	294

For the sake of comparison, the final microstructure after isothermal experiments has been examined using Scanning Electron Microscopy after nital (2 %) etching. The microstructure detailed in Table I are shown in Figure 4. Final microstructures are composed with bainite plates (B), retained austenite (A) and fresh martensite (FM). (M+B300 experiment was not considered in this analysis).

The etching is sensitive to the carbon content of the phase. The lower the carbon content, the stronger the response to etching. Bainite is thus appearing in dark contrast whereas austenite and martensite are hardly etched. Martensite shows a weak roughness and austenite remains completely smooth. At 350 °C, some transition carbides appear also in bright contrast in bainitic laths. Those observations are consistent with the HEXRD shown above and discussed later on.

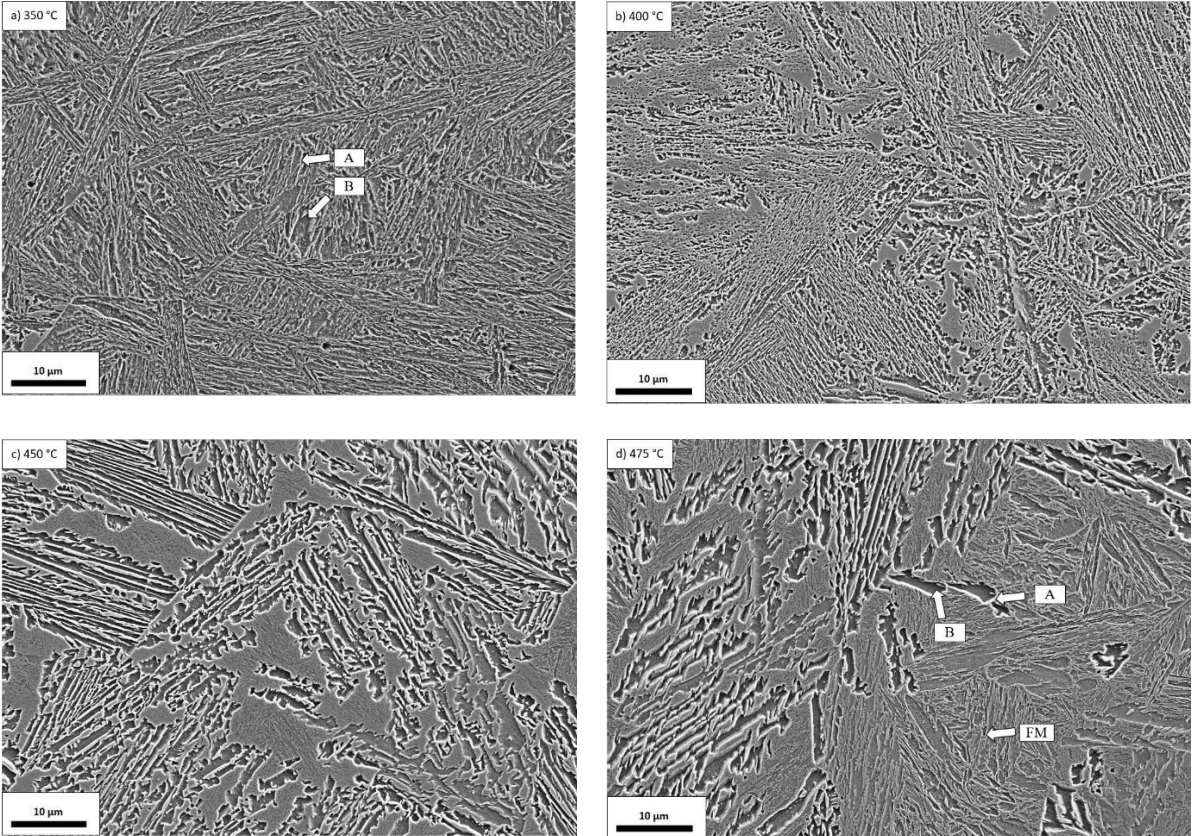


Figure 4 : SEM micrographs after nital etching 2 % of the studied steel after isothermal experiments at a) 350 °C, b) 400 °C, c) 450 °C, d) 475 °C. When possible, the microstructure components are indicated by white arrows.

Kinetics of bainite transformation in multiphased microstructures

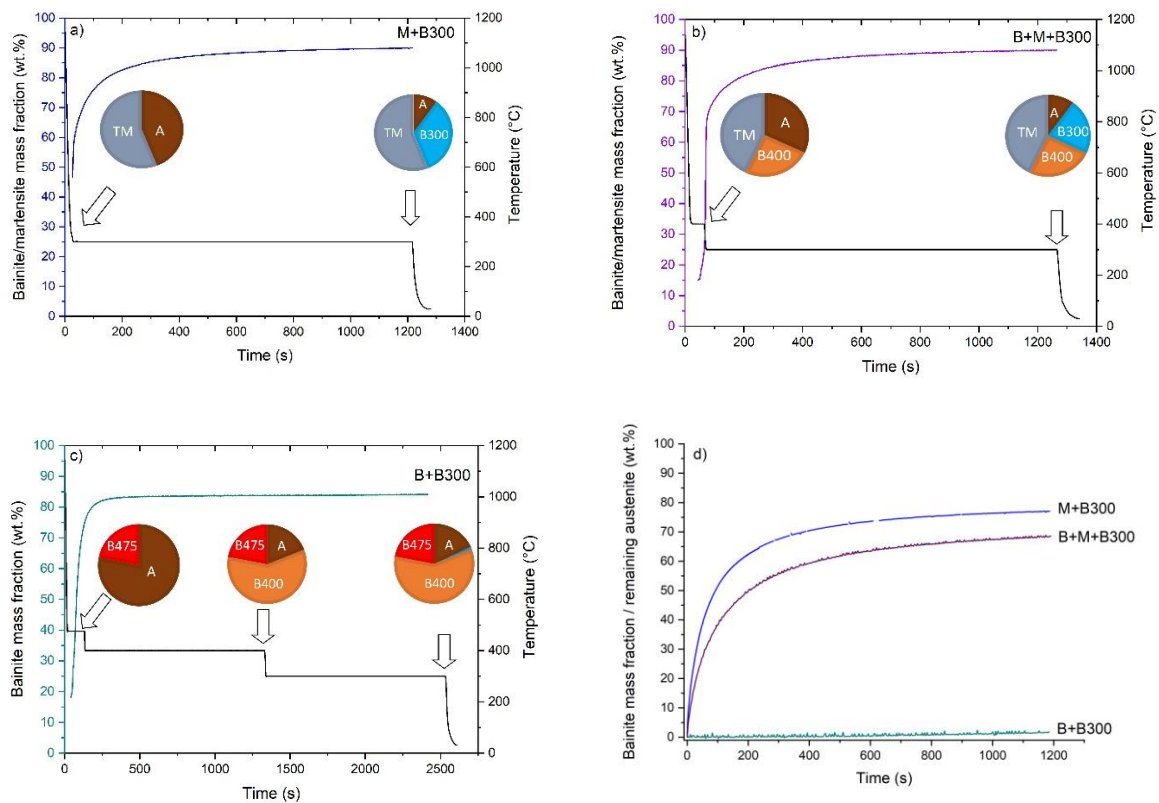


Figure 5 : Time evolutions of temperature and bainite/martensite transformation kinetics. Pie charts illustrate the composition of microstructure at different times. a) M+B300, b) B+M+B300 and c) B+B300 experiments respectively ; d) Normalized bainite kinetics in remaining austenite during the last transformation at 300 °C for M+B300, B+M+B300 and B+B300 experiments with respectively 44 wt.%, 32 wt.% and 19 wt.% of remaining austenite.

Figure 5 a), b) and c) shows the evolution of the BCT phase fraction as a function of time for the three experiments designed to study the bainite transformation below M_s , i.e. with varying starting microstructures. The temperature schedules are reported for each experiment. The expected microstructure composition at the transition between isothermal steps are represented schematically to ease the understanding of the transformation sequence. Figure 5 a) recalls the results previously discussed in Figure 3 a) for the sake of comparison.

Figure 5 b) shows the evolution of bainite mass fraction as a function of time for the B+M+B300 experiment. As for isothermal experiments, the reference time ($t = 0$) is set at the end of the austenitizing. The bainite fraction increases with time all along the two-step cooling and the bainite mass fraction exhibits a sigmoidal curve. During the first step at 400 °C, the bainite mass fraction follows the same evolution as shown previously for an isothermal transformation at the same temperature. At the end of the first step, the mass bainite fraction is 25 wt.% and stasis is obviously not reached. During the transition between 400 °C and 300 °C, a partial martensitic transformation occurs (about 43 wt.%). The bainitic transformation restarts during the second step at 300 °C but with a lower rate than at 400 °C. The fraction transformed at 300 °C is 22 wt.%. The measured fractions of austenite, martensite and bainite along the schedule are summarized in Table II. The maximal bainite and martensite mass fraction at the end of the two-step holding is equal to 90 wt.%.

Figure 5 c) shows the evolution of the bainite mass fraction as a function of time for the three-steps treatment B+B300 (green). During the first step at 475 °C, the bainite mass fraction follows the kinetics observed in isothermal transformation as shown in Figure 6. Figure 6 represents the kinetics

of bainite/martensite transformation during B+300 experiment and isothermal transformations at 475 °C, 400 °C and 300 °C. At the end of this first step, 22 wt.% of bainite at 475 °C is formed. A change in slope is observed around 120 s, this change in slope is associated with the beginning of the second step. During the second step at 400 °C, the transformation thus continues. The kinetics are slower than the ones observed during the B400 experiment alone for the corresponding fraction of bainitic ferrite formed. However, the bainite mass fraction reached at stasis during isothermal transformation of B400 is slightly higher (around 85 wt.%) than the maximal value of bainite mass fraction at stasis after a multi-step heat treatment of B+B300 (around 80 wt.%). These experiments highlight that a bainite transformation can restart at a lower temperature if the bainite fraction is not large enough. The bainite transformation thus does not respect the additivity rule as observed by Hasan et al. [39].

The estimated fractions main phases (austenite and bainite) formed during the first step at 400 °C and bainite formed during the second step are presented in Table II.

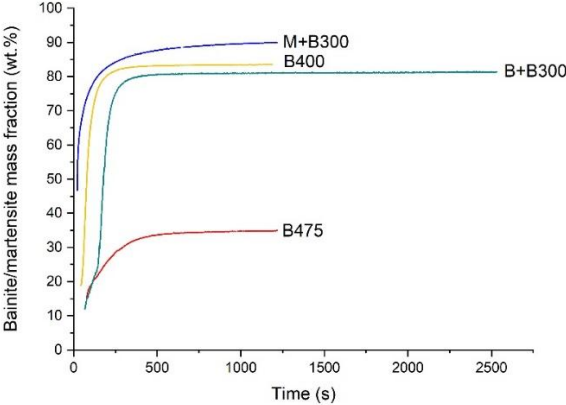


Figure 6 : Kinetics of bainite/martensite transformation during B+B300 experiments respectively (green), isothermal transformations at 475 °C (red), 400 °C (yellow) and 300 °C (blue).

Table II : Summary of the microstructures compositions (in wt.%) before and after the bainitic transformation at 300 °C (at the end of the step, before final cooling). A = Austenite, TM = Martensite, BXXX = Bainite obtained at XXX °C.

M+B300	B+M+B300	B+B300																
<table border="1"> <tr><td>A</td><td>44 %</td></tr> <tr><td>TM</td><td>56 %</td></tr> </table>	A	44 %	TM	56 %	<table border="1"> <tr><td>A</td><td>32 %</td></tr> <tr><td>TM</td><td>43 %</td></tr> <tr><td>B400</td><td>25 %</td></tr> </table>	A	32 %	TM	43 %	B400	25 %	<table border="1"> <tr><td>A</td><td>19 %</td></tr> <tr><td>B400</td><td>59 %</td></tr> <tr><td>B475</td><td>22 %</td></tr> </table>	A	19 %	B400	59 %	B475	22 %
A	44 %																	
TM	56 %																	
A	32 %																	
TM	43 %																	
B400	25 %																	
A	19 %																	
B400	59 %																	
B475	22 %																	
<table border="1"> <tr><td>A 10 %</td><td>B300 34 %</td></tr> <tr><td>TM</td><td>56 %</td></tr> </table>	A 10 %	B300 34 %	TM	56 %	<table border="1"> <tr><td>A 10 %</td><td>B300 22 %</td></tr> <tr><td>TM 43 %</td><td>B400 25 %</td></tr> </table>	A 10 %	B300 22 %	TM 43 %	B400 25 %	<table border="1"> <tr><td>A 19 %</td><td>B400 59 %</td></tr> <tr><td>B475 22 %</td><td></td></tr> </table>	A 19 %	B400 59 %	B475 22 %					
A 10 %	B300 34 %																	
TM	56 %																	
A 10 %	B300 22 %																	
TM 43 %	B400 25 %																	
A 19 %	B400 59 %																	
B475 22 %																		

Figure 5 d) shows the normalized bainite kinetics in remaining austenite during M+B300 isothermal holding (blue) and during the last step at 300 °C for the B+M+B300 (purple) and B+B300 (green) conditions respectively (see Figure 1). The reference time (t = 0) is fixed here at the beginning of the 300 °C holding for the sake of comparison. The bainite kinetics show here sigmoidal (or saturating

exponential) shapes with different saturation levels. In all cases, the bainite mass fractions however do not reach a plateau meaning that the transformation is not finished.

In isothermal conditions at M+B300 (after 56 wt.% of martensitic transformation), the transformation rate is higher than the kinetics during the holding at 300 °C in B+M+B300 condition (after 68 wt.% of B/M transformation). The fraction of bainite at 300 °C at the end of the steps are also very different (34 wt.% and 22 wt.% respectively). These results are surprising as the fractions of austenite at the beginning of the transformation are similar (44 wt.% and 32 wt.% respectively) as well as their local carbon content. For the 300 °C bainite transformation during the last step of the B+B300 cooling sequence, less than 1 wt.% of bainite formed, meaning that the transformation at 300 °C is completely inhibited in that case, permitting to maintain a higher fraction of retained austenite at the end of the step (19 wt.% instead of 10 wt.%). The conditions of stasis are thus very different compared to the two previous cases. Moreover, this highlights that bainite transformations do not respect the additivity rule.

Evolution of the tetragonality

The c and a lattice parameters of the BCT phase were obtained from the Rietveld refinement of in-situ acquired data. This measurement is not affected by the possible mechanisms disturbing the widths of the diffractions peaks; as the tetragonality is observed solely on certain diffraction peaks.

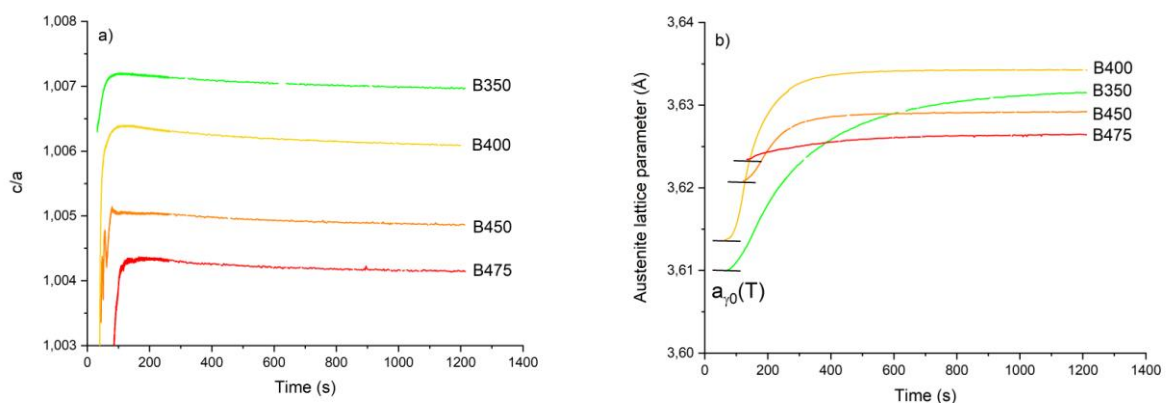


Figure 7 : a) Evolution of c/a ratio of BCT phase in isothermal conditions ; b) Evolution of the austenite lattice parameter in isothermal conditions with the $a_{\gamma 0}(T)$ the minimal austenite lattice parameter at a given temperature.

Figure 7 a) shows the evolution of c/a ratio as a function of time during isothermal holdings at temperatures between 350 °C and 475 °C. The other experiments have been excluded as it is not possible to isolate convincingly the behavior of bainite and martensite if present at the same time in the microstructure.

The changes in c/a ratio evolutions may be divided in two parts: at the beginning of the bainite transformation, the c/a ratio increases rapidly during the first 100 seconds. During the second stage, it decreases continuously while remaining above 1 (value corresponding to an ideal body-centered cubic structure). The lower the holding temperature, the higher the c/a ratio.

Austenite lattice parameter

Figure 7 b) represents the austenite lattice parameters measured by HEXRD as a function of time along isothermal holdings at temperatures between 350 °C and 475 °C. The initial values differ as the lattice parameter of stress-free austenite increases with temperature due to the thermal expansion. At the onset of isothermal holding, the austenite is assumed to represent the nominal composition.

For all studied isothermal holdings, the evolution of austenite lattice parameters show a sigmoidal shape. Hence, for all temperatures, an enrichment in carbon in austenite is observed during bainite formation if we neglect the transformation stresses.

At low temperature (350 °C), the austenite lattice parameter does not show any saturation regime at the end of the experiment (after 20 minutes). This is consistent with the transformation kinetics observed at the same temperature. The transformation still continues during the whole experiment without reaching a real stasis.

On the contrary, for B400, B450 and B475 experiments, a stasis is observed. The higher the transformation temperature, the lower the increase in the austenite lattice parameter is at the end of the holding. The carbon enrichment of austenite at stasis decreases as the temperature increases. A quantification of the carbon enrichment thanks to the Dyson and Holmes equation [40] will be discussed in the next section.

The evolution of austenite lattice parameters for transformations below M_s are analyzed and discussed in supplementary materials (Figure S1).

Discussion

Transformations above M_s

In this section, only the experiments B350 to B475 will be discussed as the microstructures along the studied isothermal holdings contain only two phases, i.e. bainite and austenite (before the final cooling during which a martensitic transformation can occur). Thanks to the measurement of the austenitic lattice parameter and the bainite tetragonality, it is possible to establish a rigorous carbon mass balance between the phases, all along the treatments. This mass balance helps characterizing, in particular, the local composition of the phases at the end of the treatment, when the transformations reach their stasis (or almost a stasis as it is the case at 350 °C). The compositions in both phases are then discussed in light of the different theories about bainitic transformations. Finally, it will be shown that the balances also permit to provide evidence that a minor fraction of carbides also precipitates during the transformation at lower temperature. This precipitation is confirmed by a careful direct observation of the diffraction patterns and of final microstructures after etching.

For the other experiments (M+B300, B+M+B300, B+B300) multiple phases are formed which jeopardizes the establishment of this balance in a reliable way.

Evolution of the carbon content in the constituting phases (bainite and austenite)

The austenite lattice parameter can be tracked all along the treatment as shown in Figure 7 b). Assuming the variation of the parameter is solely due to the carbon enrichment of austenite due to carbide-free bainitic reaction, and thus neglecting any evolution in the hydrostatic internal stress of the phase due to the displacive transformation, the carbon content in retained austenite can be calculated using the equation from Dyson and Holmes [40]:

$$C_A = C_0 + \frac{a_\gamma - a_{\gamma_0}(T)}{0.033} \quad (2)$$

where C_A and C_0 are the carbon content in retained austenite and the initial carbon content of the phase before transformation (0.27 wt.%) given in wt.% respectively, a_γ and $a_{\gamma_0}(T)$ are the austenite lattice parameter of the carbon-enriched retained austenite and the austenite lattice parameter reference before bainite transformation starts given in Å respectively. This last parameter depends

on the transformation temperature as shown in Figure 7 b). This procedure to evaluate the local composition in austenite is very common and has been exploited extensively in previous papers [2,41,42]. It is well established that carbon is not homogeneously distributed throughout the austenite. The films of retained austenite are often more enriched than blocky austenite. The carbon content measured by HEXRD appears to be a mean value.

This has been clearly demonstrated by Pushkareva et al. on two very similar alloys and transformation conditions. The final austenite carbon content measured by HEXRD have been compared to [43] direct measurements of the carbon content in austenite by EELS (Electron Energy Loss Spectroscopy); in nano-bainitic steels, Garcia-Mateo et al. [42] using APT (Atom Probe Tomography) observed a strong dispersion in carbon content values. The austenite carbon content measured by HEXRD is a mean value taking into account the film-like austenite carbon-rich and blocky austenite carbon-poor, an closer to these last values. As done by some authors [2,44], the heterogeneity of carbon content can be estimated taking into consideration two austenite phases in the Rietveld refinement procedure.

The fact the HEXRD leads to mean carbon content measurement close to the ones that could be given by EELS or by APT sustains the hypothesis that the hydrostatic stresses do not play a major role in the evolution of the lattice parameter of austenite during the bainitic transformation and do not affect in turn the measurement of carbon content. It must be mentioned that it is not the case if the bainitic transformation is preceded by a martensitic transformation, as is it the case of Q&P steels [45,46].

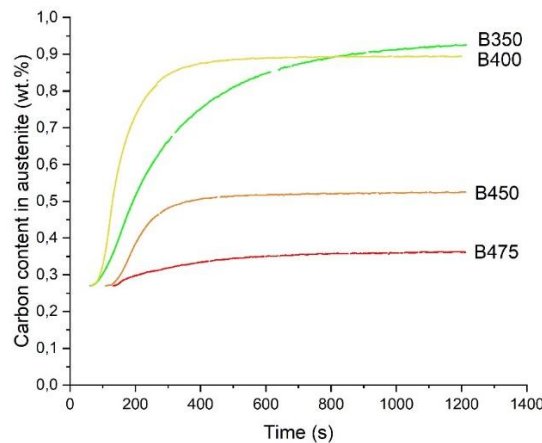


Figure 8 : Carbon content in retained austenite as a function of time during the isothermal holdings between 350 °C and 450 °C, determined by the procedure detailed in the text (nominal carbon content 0.27 wt.%).

Figure 8 shows the evolution of the carbon content in austenite determined according to the procedure described above. As expected, the carbon content increases in all cases following sigmodal curves, i.e. with a rapid initial enrichment starting from the nominal carbon content (0.27 wt.%) then followed by a plateau. It must be emphasized that the plateau/stasis is not reached for B350 experiment. For the experiments having reached the plateau, the carbon content in austenite at the plateau decreases with temperature. This trend is consistent with the fraction of retained austenite at stasis assuming a first-order carbon balance.

$$C_A = \frac{C_0}{F_A} \quad (3)$$

The higher the fraction of retained austenite, the lower the enrichment is. This last equation supposes a complete partition of carbon between bainite and austenite. However, this too simple equation cannot hold. For B400 at stasis, the fraction of retained austenite is 17 wt.% meaning that the expected carbon content should be 1.76 wt.% instead of 0.89 wt.%. It thus means that a

significant fraction of carbon remains in fact trapped in bainitic ferrite, which, in turn, explains the tetragonality of the ferritic lattice shown in previous Figure 7 b).

According to the Zener ordering theory [47], the carbon atoms in solid solution in a ferritic lattice tend to segregate collectively to certain octahedral sites of the BCC lattice and distort it. It is commonly admitted that a BCT structure is then obtained. The distortion of the lattice was shown to be proportional to the carbon content in solid solution. As in previous published works on bainitic and martensitic steels, the carbon content in bainite can be estimated on the basis of the tetragonality as followed [2,48–51]:

$$\frac{c}{a} = 1 + 0.045 C_B \quad (4)$$

where C_B is the concentration of carbon in wt.%.

In the literature, it is not clear if this estimation of the carbon content also encompasses carbon clusters or carbon segregated at defects, such as dislocations or bainitic lath boundaries [19,52]. Moreover, it must be mentioned that the recent works of Maugis et al. show that the distortion due to Zener's ordering could also lead to an orthorhombic lattice under a compressive stress state (tetragonal in tension) [53,54]. It could explain why an even better agreement can be obtained with an orthorhombic lattice to model diffraction peaks [28].

As a consequence, the estimated carbon content in bainite follows the trends illustrated in Figure 7 a) if Equation (4) applies. For the four isothermal experiments above M_s , the carbon content first increases rapidly and decrease smoothly after about 100 s. The rapid increase must not be interpreted as the fraction of bainite is low and the uncertainty about the tetragonality measurement is too high. However, the trends after 100 s are more relevant. The lower the transformation temperature is, the higher the carbon content in bainite (from 0.09 wt.% at 450 °C up to 0.15 wt.% at 350 °C at the end of the experiments). These high values are consistent with the values reported in the literature in similar alloys and were used to support the diffusionless theory [28,30] of bainitic transformation. At the beginning of transformation, supersaturated bainite nucleates with a carbon content equal to the prior austenite. During the transformation process, the c/a ratio decreases by partitioning.

Carbon mass balance at the end of the isothermal holding

Table III summarizes the phase fractions and carbon contents at the end of isothermal experiments at temperatures above M_s . The isothermal transformation at 300 °C (M+B300) has been discarded as it is difficult to deconvolute correctly the effect of prior martensite transformation on the carbon content in bainite. Moreover, for this particular experiment, the transformation is far from having reached a stasis. The first column contains the temperature of isothermal holding. The second and the fourth columns contain the bainite mass fraction F_B (wt.%) and the austenite mass fraction F_A (wt.%) determined by Rietveld refinement respectively. The third column shows the C_B in wt.% corresponding to the carbon content in bainite obtained thanks to the tetragonality factor c/a at the end of the isothermal holding using equation 1.

Table III : Phase fractions and carbon contents measured by HEXRD at the end of holdings, the estimated ΔC by a simple carbon mass balance.

Isothermal temperature (°C)	Bainite mass fraction (wt.%) F_B	Bainite carbon content (wt.%) C_B	Austenite mass fraction (wt.%) F_A	Austenite carbon content (wt.%) C_A	ΔC
350	90	0.15	10	0.92	0.03
400	84	0.14	16	0.89	0.01
450	60	0.11	40	0.52	0.00
475	35	0.09	65	0.36	0.00

The last column contains the carbon deficit, ΔC , calculated as:

$$C_0 = C_B F_B + C_A F_A + \Delta C \quad (5)$$

where C_0 is the nominal carbon content in the steel grade. This function ΔC represents the carbon not found in austenite and in bainite by the independent determination of the carbon trapped in each phase. ΔC is thus thought to represent the carbon trapped in carbides.

The mathematical error in the Rietveld procedure for the determination of the phase fractions is ± 1 wt.%. On the contrary the relative error on the measurement of the austenite lattice parameter is low ($2 \cdot 10^{-4}$). The errors made on the tetragonality are more difficult to evaluate as it could depend on the way in which the width of diffraction peaks is modeled. Moreover, the determination of C_B using the tetragonality of the BCT lattice can be discussed [49]. Nevertheless, the high degree of confidence on the phase fraction and lattice parameter of austenite leads to the same conclusion that a significant part of the carbon content remains in fact trapped in bainite. The order of magnitude of the carbon content out of austenite ($C_B F_B + \Delta C$) would have given similar C_B values between 0.2 wt.% and 0.1 wt.%. These values are indubitably higher than the values expected in a BCC phase after a transformation under paraequilibrium.

In the following, the values presented in Table III (carbon composition of austenite and bainite at the end of the experiments) will be discussed in light of diffusionless theory for carbide-free bainitic transformation. Finally, the very low residual fraction of carbon ΔC will be shown to be explained by the presence of carbides (precipitated carbon). In the Rietveld refinement procedure, only austenite and bainite are considered. Nevertheless, the fraction of precipitates remains very low (far below the experimental resolution) and doesn't affect the fraction measured above.

Carbon in austenite and validity of T_0' criterion

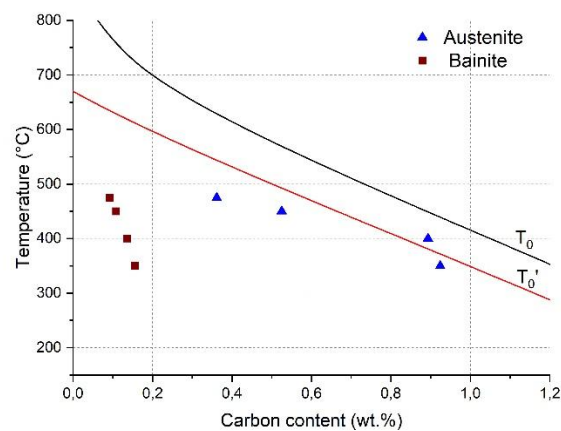


Figure 9 : Carbon content in retained austenite (triangles) and in bainite (squares) for isothermal conditions (T_0 and T_0' lines).

The carbon contents in retained austenite at the end of studied isothermal holdings are shown in Figure 9. These values are compared with the T_0 and T_0' lines calculated with *Thermocalc* software and TCFE9 database. These lines represent the supposed thermodynamic limits for bainite nucleation assuming the equality of the Gibbs energy of BCC ferrite (representing bainite) and austenite. The T_0' line also takes into account an additional elastic strain energy of 400 J/mol in the ferrite in accordance with the diffusionless theory of Bhadeshia [13].

Experimental austenite carbon contents are close to the T_0' line only at the lower transformation temperatures (B400 and B350 experiments). For the latter, the transformation was shown to not have reached the stasis (transformation time is too short). The value presented here is thus low compared to the value really expected at stasis. On the contrary, at high temperatures (B450 and B475 experiments) the values are far from the T_0' line even if the kinetics show a clear stasis in the transformation (cf. Figure 3 a)). Such discrepancy between experiment and T_0' line at high temperatures has also been reported by some groups [2,8,55]. The T_0' criterion seems thus to be validated at low temperature but is clearly not verified at high temperatures.

Carbon supersaturation in bainite

The carbon contents in bainite obtained at the end of our isothermal experiments are represented by red squares (values found in Table III) in Figure 9.

The recent criterion assuming the equality of the Gibbs energy of a BCT phase (representing more convincingly bainite) and austenite proposed by Ranjan et al. [55] could explain why the carbon content in austenite could exceed the conventional T_0' line at the lower temperatures. On the contrary, at high temperatures, the new criterion cannot explain why the stasis is reached sooner than expected from the criterion.

For the sake of comparison, the values obtained on similar alloys after isothermal holdings by Pushkareva et al. [56], Garcia-Mateo et al. [29] and by Ranjan et al. [55] have been compared with our values. Pushkareva et al. [56] have measured the carbon content in bainitic laths by EELS (Electron Energy Loss Spectroscopy) whereas Garcia-Mateo et al. [29] and Ranjan et al. [55] have used APT (Atom Probe Tomography).

The lower the temperature, the higher the carbon content in bainite is. Those results are in agreement with results from the literature [29,32,55–57]. Ranjan et al. [55] have explained recently this evolution by a correlation with the austenite carbon content which also increases.

As already discussed, these values are high compared to the carbon solubility in BCC phase and supports according to [55] the diffusionless theory of bainitic transformation. These results for all the isothermal experiments plead in favor of a bainite formed at low temperature following the lower bainite description of Bhadeshia [13]. Carbon remains trapped in bainite at low temperature since the diffusion of carbon is slow at low temperature. CFB obtained in isothermal conditions is thus highly supersaturated in carbon and its carbon content depends on the transformation temperature.

Carbides

The ΔC values identified in Table III represent the carbon missing in solid solution in bainite and in austenite. The values found are weak (max. 10 wt.% of the nominal carbon content) and decrease with increasing transformation temperatures. Above 400 °C, the values are negligible considering the precision of the measurement.

If solid solution is set aside, the other possible mechanisms able to trap carbon are numerous: segregations on dislocations, segregations on lath/blocks/packet boundaries, local enrichment in austenite or precipitation of carbides. In the literature, it is not well established whether the carbon segregates on defects also contributes to the obvious tetragonality observed on the bainitic phase [19,58].

The presence of carbides is the better explanation found to explain the ΔC values at low transformation temperatures (mainly at 350 °C). In fact, carbides can also be directly evidenced by SEM observations and by looking carefully at diffractograms as shown in Figure S2. of the supplementary materials. At 350°C, the transition carbides mass fraction is estimated less than 1 wt.% using a manual refinement (the uncertainty in phase fraction obtained by the Rietveld refinement is ± 1 wt.%), value that is consistent with the one obtained by the carbon mass balance. As a consequence, it is not possible to decide if the whole ΔC value can be explained by these carbides.

It must be mentioned that the steel contains around 0.1 wt.% of sulfur. As a consequence, it contains a large fraction of MnS which is well highlighted on the diffractograms in Figure S2 of the supplementary materials (cyan boxes). Even if the studied steel present a large fraction of MnS, the mean Mn composition in the matrix is not affected (no effect on M_s and T_0 lines). On the diffraction patterns, there is no overlapping peaks between MnS, transition carbides and cementite.

Transformation below M_s

In this section, we discuss the outcomes of the “step treatments”, which include as a last step an isothermal treatment at 300 °C, below the M_s , during which a bainite transformation will take place. We compare the kinetics of the bainite transformation as a function of starting microstructure, as recalled in Table II. As shown in Figure 5, the bainite transformation kinetics at 300 °C are drastically different among the three experiments, despite a significant amount of austenite remaining to be transformed in all cases.

These differences in kinetics can be interpreted qualitatively. The kinetics of M+B300 are fastest because the initial austenite fraction is the highest and because the austenite did not have time to get enriched in carbon during the martensitic transformation down to 300 °C. According to previous works [33,37], the new martensite/austenite interfaces also provide nucleation sites, which accelerate the bainite transformation.

For the experiment B+B300, the kinetics are the slowest (almost no detectable bainite transformation) because it has the lowest amount of austenite in the initial microstructure and the austenite got enriched by carbon (0.93 wt.%). The kinetics of B+M+B300 experiment are intermediate because there are more austenite remaining than to the latter experiment, it are less enriched in carbon (0.91 wt.%) and the martensite provides new nucleation sites.

Accordingly, the austenite fraction at the end of the bainite transformation at 300 °C is the highest for the B+B300 treatment. Let us mention that the final carbon concentration is quasi similar among the two experiments (Table IV), showing that the final stasis is not simply related to this parameter. The previously formed microstructure modifies the carbon mass balance and therefore the final fraction of austenite.

Hence, these experiments show that the overall bainite transformation is not simply linked with the temperature and the fraction of already-formed bainite (i.e. it is not additive): it depends on the already formed microstructure, which is itself dependent on the previous thermal history. This conclusion is in agreement with previous investigations by Hasan et al. [39]. The non-additivity is already highlighted above the M_s temperature in Figure 6. Put together, these results are in agreement with previous studies which recently demonstrated that multi-step cooling sequences are more efficient to stabilize retained austenite at room temperature than conventional single isothermal treatments [39,59,60]. This is of both practical and industrial interest [1,4], even if its origin remains poorly understood.

Table IV : Austenite mass fractions and carbon contents measured by HEXRD at the end of the last step of multi-step cooling sequences.

Cooling sequence	Temperature (°C)	Austenite mass fraction (%)	Austenite carbon content (wt.%)
B+M+B300	300	10	0.91
B + B300	300	19	0.93

Table IV is a summary of austenite fractions and austenite carbon contents at the end of the last step at 300 °C for the B+M+B300 and B+B300 cooling sequence. As presented before, austenite mass fraction transformed depend of the schedule. A higher fraction of retained austenite is measured at the end of the B+B300 treatment. Even if, the austenite carbon content at the end of the final step is very close for both multi-step treatment. Hence, the retained austenite fraction and carbon composition depend on the transformation history. Both are the key to understand the mechanical performance of these microstructures and sustain their industrial interest [1,4].

Conclusions

Bainite transformations were investigated by in-situ High energy X-Ray diffraction above and below M_s temperature. These experiments have permitted to determine with good accuracy the bainite kinetics transformation along isothermal and multi-step cooling sequences. The composition of phases are tracked using the determination of the austenite lattice parameter and the tetragonality of bainite lattice. At the end of isothermal holdings, a carbon enrichment is observed in austenite despite high carbon content trapped in bainite (in particular for low temperature conditions). The

austenite carbon content at the end of the holding was compared to the displacive criterion T_0' line. The experimental values are close to the T_0' line however this criterion is not respected for high temperature transformation. For transformations above M_s , a precise carbon mass balance is proposed highlighting carbide formation at the lowest temperature. For transformations below M_s , the bainite transformation is dependent on the history and previous transformations. This sensitivity has been explained in term of austenite stability and nucleation processes. The bainite transformation does not thus respect the additivity rule.

Acknowledgements

This work was supported by Ascometal (CREAS) Hagondange. The synchrotron experiments were realized in 2018 under the project I-20180850 EC at DESY PETRA III in Hamburg. The authors would like to thank the team of P07 line, in particular Norbert Schell and Andreas Stark. Their expertise in very was much appreciated and widely contributed to the success of the study.

Financial relationship

This work was funded by Ascometal, Swiss steel group, by the Université de Lorraine, by the CNRS (Centre de la Recherche Scientifique) and the French ANRT (Agence National de la Recherche et de la Technologie) under the CIFRE convention (2018/1307). The HEXRD experiments were conducted at DESY (PETRA III-P07 beamline) in Hamburg.

Conflicts of Interest

The authors declare that they have no conflict of interest.

References

1. F. G. Caballero, S. Allain, J. Cornide, J. D. Puerta Velásquez, C. Garcia-Mateo, and M. K. Miller, *Mater. Des.* **49**, 667 (2013).
2. L. Guo, H. K. D. H. Bhadeshia, H. Roelofs, and M. I. Lembke, *Mater. Sci. Technol.* **33**, 2147 (2017).
3. H. I. Aaronson, W. T. Reynolds, and G. R. Purdy, *Metall. Mater. Trans. A* **37**, 1731 (2006).
4. T. Sourmail, *HTM J. Heat Treat. Mater.* **72**, 371 (2017).
5. T. Sourmail, C. Garcia-Mateo, F. Caballero, L. Morales-Rivas, R. Rementeria, and M. Kuntz, *Metals* **7**, 31 (2017).
6. B. C. De Cooman, *Curr. Opin. Solid State Mater. Sci.* **8**, 285 (2004).
7. W. T. Reynolds, F. Z. Li, C. K. Shui, and H. I. Aaronson, *Metall. Trans. A* **21**, 1433 (1990).
8. H.-D. Wu, G. Miyamoto, Z.-G. Yang, C. Zhang, H. Chen, and T. Furuhashi, *Acta Mater.* **133**, 1 (2017).
9. Santajuana, Eres-Castellanos, Ruiz-Jimenez, Allain, Geandier, Caballero, and Garcia-Mateo, *Metals* **9**, 925 (2019).
10. M. Y. Sherif, C. G. Mateo, T. Sourmail, and H. K. D. H. Bhadeshia, *Mater. Sci. Technol.* **20**, 319 (2004).
11. J.-C. Hell, M. Dehmas, S. Allain, J. M. Prado, A. Hazotte, and J.-P. Chateau, *ISIJ Int.* **51**, 1724 (2011).
12. F. G. Caballero and H. K. D. H. Bhadeshia, *Curr. Opin. Solid State Mater. Sci.* **8**, 251 (2004).
13. H. K. D. H. Bhadeshia, *Bainite in Steels: Transformations, Microstructure and Properties*, 2. ed (IOM Communications, London, 2001).
14. Z. Tournoud, *Caractérisation Multi-Échelle d'un Acier Bainitique Microallié à Effet TRIP*, PhD Thesis, Université Grenoble Alpes (ComUE), 2019.
15. L. C. D. Fielding, *Mater. Sci. Technol.* **29**, 383 (2013).
16. A. M. Ravi, J. Sietsma, and M. J. Santofimia, *Acta Mater.* **105**, 155 (2016).
17. D. Quidort and Y. J. M. Brechet, *Acta Mater.* **49**, 4161 (2001).
18. S. Allain, S. Aoued, A. Quintin-Poulon, M. Gouné, F. Danoix, J.-C. Hell, M. Bouzat, M. Soler, and G. Geandier, *Materials* **11**, 1087 (2018).
19. R. Rementeria, J. A. Jimenez, S. Y. P. Allain, G. Geandier, J. D. Poplawsky, W. Guo, E. Urones-Garrote, C. Garcia-Mateo, and F. G. Caballero, *Acta Mater.* **133**, 333 (2017).
20. (n.d.).
21. S. M. C. van Bohemen, *Mater. Sci. Technol.* **28**, 487 (2012).
22. A. Nehrenberg, *Trans. AIME* **167**, 494 (1946).
23. D. Forgeoux, *Application Des Structures Bainitiques Par Transformation Isotherme et d'un Traitement de Surface Adapté Aux Vis à Haute Résistance*, Theses, Université de Technologie de Belfort-Montbéliard, 2016.
24. G. Ashiotis, A. Deschildre, Z. Nawaz, J. P. Wright, D. Karkoulis, F. E. Picca, and J. Kieffer, *J. Appl. Crystallogr.* **48**, 510 (2015).
25. H. M. Rietveld, *J. Appl. Crystallogr.* **2**, 65 (1969).
26. J. Rodríguez-Carvajal, *Phys. B Condens. Matter* **192**, 55 (1993).
27. B. H. Toby, *Powder Diffr.* **21**, 67 (2006).
28. C. N. Hulme-Smith, I. Lonardelli, A. C. Dippel, and H. K. D. H. Bhadeshia, *Scr. Mater.* **69**, 409 (2013).
29. C. Garcia-Mateo, J. A. Jimenez, H.-W. Yen, M. K. Miller, L. Morales-Rivas, M. Kuntz, S. P. Ringer, J.-R. Yang, and F. G. Caballero, *Acta Mater.* **91**, 162 (2015).
30. C. N. Hulme-Smith, M. J. Peet, I. Lonardelli, A. C. Dippel, and H. K. D. H. Bhadeshia, *Mater. Sci. Technol.* **31**, 254 (2015).
31. H. K. D. H. Bhadeshia, *Philos. Mag.* **93**, 3714 (2013).
32. J. H. Jang, H. K. D. H. Bhadeshia, and D.-W. Suh, *Scr. Mater.* **68**, 195 (2013).
33. A. Navarro-López, J. Hidalgo, J. Sietsma, and M. J. Santofimia, *Mater. Charact.* **128**, 248 (2017).
34. A. Navarro-López, J. Sietsma, and M. J. Santofimia, *Metall. Mater. Trans. A* **47**, 1028 (2016).
35. D. Kim, S.-J. Lee, and B. C. De Cooman, *Metall. Mater. Trans. A* **43**, 4967 (2012).

36. S. M. C. van Bohemen, M. J. Santofimia, and J. Sietsma, *Scr. Mater.* **58**, 488 (2008).
37. A. M. Ravi, A. Navarro-López, J. Sietsma, and M. J. Santofimia, *Acta Mater.* **188**, 394 (2020).
38. W. Steven, *J. Iron Steel Inst.* **183**, 349 (1956).
39. S. M. Hasan, S. Kumar, D. Chakrabarti, and S. B. Singh, *Philos. Mag.* **100**, 797 (2020).
40. D. J. DYSON, *J. Iron Steel Inst* **208**, 469 (1970).
41. P. Jacques, E. Girault, T. Catlin, N. Geerlofs, T. Kop, S. van der Zwaag, and F. Delannay, *Mater. Sci. Eng. A* **273–275**, 475 (1999).
42. C. Garcia-Mateo, F. G. Caballero, M. K. Miller, and J. A. Jimenez, *J. Mater. Sci.* **47**, 1004 (2012).
43. I. Pushkareva, B. Shalchi-Amirkhiz, S. Y. P. Allain, G. Geandier, F. Fazeli, M. Sztanko, and C. Scott, *Metals* **10**, 392 (2020).
44. S. S. Babu, E. D. Specht, S. A. David, E. Karapetrova, P. Zschack, M. Peet, and H. Bhadeshia, *Metall. Mater. Trans. A* **36**, 3281 (2005).
45. S. Allain, G. Geandier, J.-C. Hell, M. Soler, F. Danoix, and M. Gouné, *Metals* **7**, 232 (2017).
46. S. Y. P. Allain, S. Gaudez, G. Geandier, J.-C. Hell, M. Gouné, F. Danoix, M. Soler, S. Aoued, and A. Poulon-Quintin, *Mater. Sci. Eng. A* **710**, 245 (2018).
47. C. Zener, *Trans Aime* **167**, 550 (1946).
48. J. W. Christian, *Mater. Trans. JIM* **33**, 208 (1992).
49. Y. Lu, H. Yu, and R. D. Sisson, *Mater. Sci. Eng. A* **700**, 592 (2017).
50. Z. Nishiyama, *Martensitic Transformation* (Elsevier, 2012).
51. C. S. Roberts, *JOM* **5**, 203 (1953).
52. R. Rementeria, J. D. Poplawsky, M. M. Aranda, W. Guo, J. A. Jimenez, C. Garcia-Mateo, and F. G. Caballero, *Acta Mater.* **125**, 359 (2017).
53. P. Maugis, *Comput. Mater. Sci.* **159**, 460 (2019).
54. P. Maugis, D. Connétable, and P. Eyméoud, *Scr. Mater.* **194**, 113632 (2021).
55. R. Ranjan and S. B. Singh, *Acta Mater.* **202**, 302 (2021).
56. I. Pushkareva, B. Shalchi-Amirkhiz, S. Y. P. Allain, G. Geandier, F. Fazeli, M. Sztanko, and C. Scott, *Metals* **10**, 392 (2020).
57. F. G. Caballero, M. K. Miller, C. Garcia-Mateo, J. Cornide, and M. J. Santofimia, *Scr. Mater.* **67**, 846 (2012).
58. F. G. Caballero, M. K. Miller, and C. Garcia-Mateo, *Acta Mater.* **58**, 2338 (2010).
59. J. Tian, G. Xu, Z. Jiang, M. Zhou, H. Hu, and Q. Yuan, *ISIJ Int.* **58**, 1875 (2018).
60. X. L. Wang, K. M. Wu, F. Hu, L. Yu, and X. L. Wan, *Scr. Mater.* **74**, 56 (2014).